JACS
JOURNAL OF THE AMERICAN CHEMICAL SOCIETY

Article

pubs.acs.org/JACS

Understanding the Effect of Fluorocarbons in Aqueous Supramolecular Polymerization: Ultrastrong Noncovalent Binding and Cooperativity

Elisha Krieg,[†] Haim Weissman,[†] Eyal Shimoni,[‡] Alona Bar On (Ustinov),[†] and Boris Rybtchinski*[,†]

Departments of [†]Organic Chemistry and [‡]Chemical Research Support, Weizmann Institute of Science, Rehovot 76100, Israel

Supporting Information

ABSTRACT: Achieving supramolecular polymerization based on strong yet reversible bonds represents a significant challenge. A solution may be offered by perfluoroalkyl groups, which have remarkable hydrophobicity. We tested the idea that a perfluorooctyl chain attached to a perylene diimide amphiphile can dramatically enhance the strength of supramolecular bonding in aqueous environments. Supramolecular structures and polymerization thermodynamics of this fluorinated compound (**1-F**) were studied in comparison to its non-fluorinated analogue (**1-H**). Depending on the amount of organic cosolvent, **1-F** undergoes cooperative or isodesmic aggregation. The switching between two polymerization mechanisms results from a change in polymer structure, as observed by cryogenic electron microscopy. **1-F** showed exceptionally strong noncovalent binding, with the largest directly measured association constant of 1.7×10^9 M^{-1} in 75:25 water/THF mixture (v/v). In pure water, the association constant of **1-F** is estimated to be at least in the order of 10^{15} M^{-1} (based on extrapolation), 3 orders of magnitude larger than that of **1-H**. The difference in aggregation strength between **1-F** and **1-H** can be explained solely on the basis of the larger surface area of the fluorocarbon group, rather than a unique nature of fluorocarbon hydrophobicity. However, differences in aggregation mechanism and cooperativity exhibited by **1-F** appear to result from specific fluorocarbon conformational rigidity.

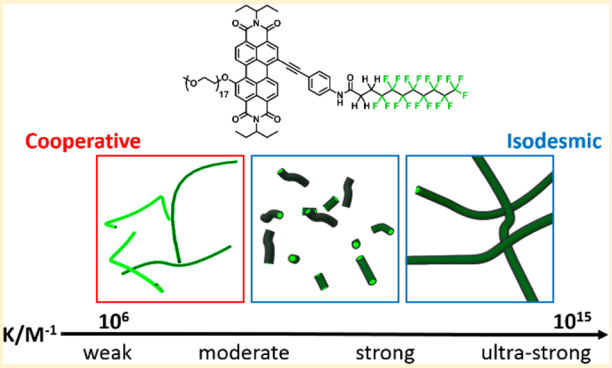

INTRODUCTION

Supramolecular polymerization is an emerging process for creating noncovalent nanostructures pertinent to materials applications.[1−5] The reversible intermolecular binding in supramolecular polymers gives rise to adaptive properties that are fundamentally different from those of conventional polymer materials, enabling stimuli-responsiveness, self-healing properties, and advantages in processing and recycling. Supramolecular polymerization also plays an important role in living systems, for instance in the formation of actin filaments and microtubules.

Achieving strong yet reversible binding in synthetic supramolecular polymers is crucial, since the average length and mechanical stability of the polymer chains are determined by the association constants of aggregation. The polymer size distribution is also influenced by the aggregation mechanism:[6] simple isodesmic aggregation yields moderate chain lengths, whereas under similar conditions, cooperative (nucleation−elongation) mechanisms produce long chains that are in equilibrium with the monomer molecules.[7,8] Due to the inherent weakness of noncovalent bonds, it remains challenging to develop supramolecular polymers that do not break apart at high temperatures or in dilute solutions, while retaining their dynamic properties. This lack of stability is a major obstacle for practical application.

In their seminal paper, Meijer and co-workers showed that strong association between self-complementary 2-ureido-4-pyrimidone groups afforded supramolecular polymers with large molecular weight.[9] The association constant (K) is very high in toluene ($K = 6 \times 10^8$ M^{-1}) and in other organic solvents, but becomes weak in the presence of water.[10] Aida and co-workers have reported formation of very long helical supramolecular polymers composed of hexabenzocoronene-based Gemini amphiphiles.[11,12] Other examples of remarkably stable supramolecular polymers include systems based on $\pi-\pi$ interactions between large polycyclic aromatic molecules (reported association constants of up to $\sim 10^8$ M^{-1})[13] and a self-complementary zwitterion motif ($K \geq 10^{10}$ M^{-1}).[14,15] The supramolecular polymers with the highest reported association constants are based on metal−ligand interactions stabilized by chelate effects, where values of up to $K \approx 10^{14}$ M^{-1} (in Fe(II) terpyridine complexes)[16] are reached.

Another strategy to create very strong noncovalent binding is based on the use of hydrophobic interactions.[17−20] Understanding and controlling supramolecular polymerization in aqueous medium is particularly important, due to the role of water in biological self-assembly,[21] and due to its availability,

Received: April 18, 2014
Published: June 10, 2014

dx.doi.org/10.1021/ja503906p | J. Am. Chem. Soc. 2014, 136, 9443−9452

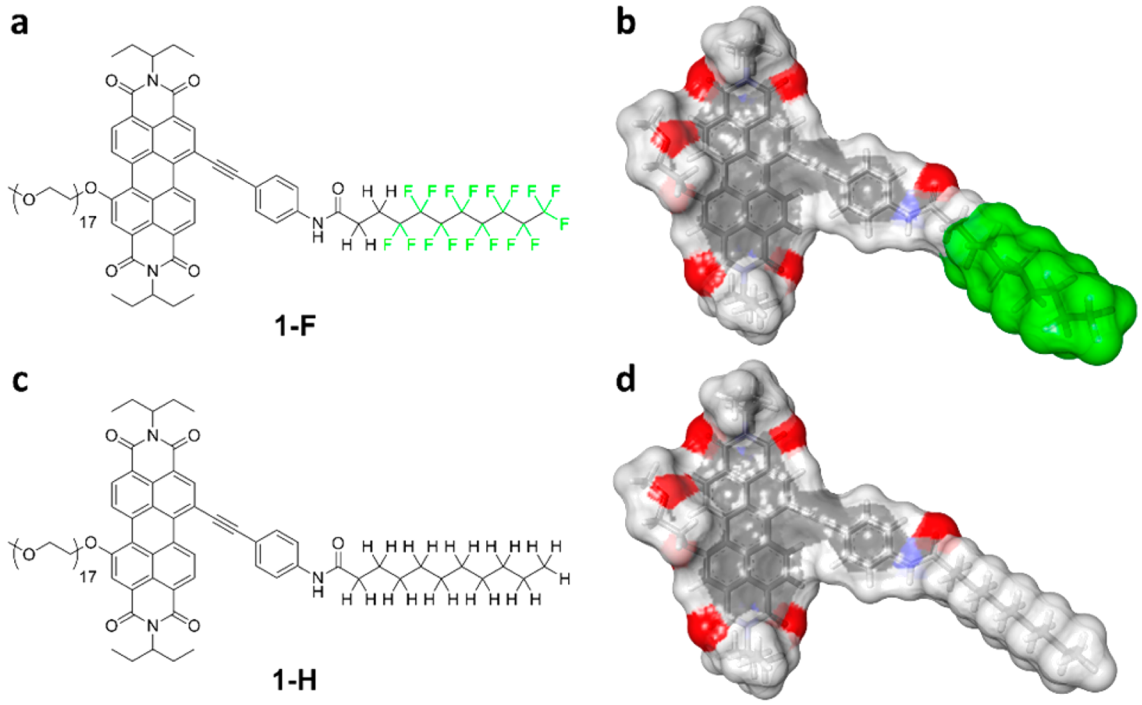

Figure 1. Compounds **1-F** and **1-H**. (a) Chemical structure of **1-F** and (b) its solvent-accessible surface (the perfluorooctyl chain is highlighted in green). (c) Chemical structure of **1-H** and (d) its solvent-accessible surface. The molecular models were obtained from geometry optimization by the semiempirical PM6-DH+ method (see Supporting Information). For simplification, PEG chains are modeled as $-O(CH_2-CH_2)OCH_3$ groups.

low cost, and environmental safety. The strength of the hydrophobic effect steeply grows with increasing size of the hydrophobic surface.[22−24] Our group has reported several supramolecular polymers composed of amphiphilic molecules having extended π-surfaces.[18,25−27] These large molecular surfaces were constructed from perylene diimide (PDI) groups, which are advantageous building blocks in supramolecular chemistry, exhibiting strong aggregation, especially in water.[28,29] The combination of multiple PDI groups ensured very strong binding (e.g., $K = 8 \times 10^8$ in 70:30 water/THF (v/v)),[27] and one system was stable enough to be used as an ultrafiltration membrane.[30] In these systems, the exceedingly strong hydrophobic bonding in pure water precluded the direct measurement of the association constants, limiting the assessment of noncovalent bond strength. The latter is of fundamental importance for understanding hydrophobic interactions and developing new materials.

The present study aimed at developing a highly stable noncovalent polymer based on hydrophobic interactions, and characterizing its thermodynamic stability and structure. Instead of further increasing the number of hydrophobic π-conjugated moieties, we wished to study the effect of a perfluorinated alkyl chain (F-chain) attached to a single PDI group. F-chains have unique properties, very different from those of hydrocarbons (H-chains). In particular, they are more stable, bulkier, stiffer, lipophobic, and significantly more hydrophobic.[31,32] Amphiphiles furnished with F-chains have slower aggregation kinetics, different packing parameters, and much smaller critical aggregation concentrations than their H-chain analogues.[32] Notably, the unique nature of F-chain hydrophobicity has been disputed.[32,33] Recent computational studies have suggested that the strong hydrophobicity of F-chains originates from their bulkiness and less efficient packing.[34] Whitesides and co-workers have shown that the hydrophobic binding of short F-chains to the hydrophobic cavity of carbonic anhydrase is indistinguishable from that of H-chains when correcting for solvent-accessible surface.[35]

Herein we report the structure and thermodynamic properties of a supramolecular polymer based on F-chain-functionalized PDI amphiphile **1-F** (Figure 1a,b), as compared to its non-fluorinated analogue **1-H** (Figure 1c,d). In order to test the impact of the F-chain on morphology, aggregation mechanism, and thermodynamic stability, we combined electron microscopic imaging with temperature- and concentration-dependent thermodynamic studies. We found that the polymerization of **1-F** into very long nanofibers involves exceptionally strong, noncovalent binding and exhibits profound changes in aggregation mechanism and morphology, which are not observed in **1-H**.

RESULTS AND DISCUSSION

Design Concept. Compound **1-F** was designed to yield highly stable supramolecular nanostructures in aqueous medium (Figure 1a). The molecule comprises an extended π-conjugated surface based on PDI that brings about strong intermolecular $\pi-\pi$/hydrophobic interactions.[28] PDI shows distinct spectral changes upon aggregation that enable spectroscopic investigation of the aggregation processes.[36,37] An aniline amide group served as a linker to attach a perfluorooctyl chain, and a C_2H_4 spacer separated the amide group from the electron-withdrawing fluorocarbon group. The aniline amide is prone to undergo H-bonding, serving as both H-bond donor and acceptor. Although H-bonds generally become weak in aqueous medium, it is known that they can retain their strength in a hydrophobic microenvironment (e.g., when located between large hydrophobic groups).[20,38,39] Finally, the hydrophilic poly(ethylene glycol) (PEG) chain provides solubility in aqueous medium. We also prepared the

dx.doi.org/10.1021/ja503906p | J. Am. Chem. Soc. 2014, 136, 9443−9452

non-fluorinated analogue **1-H**, which served as a reference system (Figure 1c). Both molecules are readily prepared in two steps with high yields from a previously reported PDI precursor[25] and commercially available compounds (see Supporting Information).

Figure 1b,d shows the solvent-accessible surface (SAS) areas of **1-F** and **1-H**. As a result of the bulkiness of the perfluorooctyl group, the hydrophobic surface of **1-F** is larger than that of **1-H**. The difference is estimated to be 87 Å^2 based on the SAS[40] or 68 Å^2 based on the solvent-excluded surface (SES).[41] In both compounds the H-bonding and $\pi-\pi$/hydrophobic interactions imposed by the aromatic core were expected to determine the direction of supramolecular polymerization, whereas the linear alkyl or fluoroalkyl chains increased the overall hydrophobicity.

Aggregation in Aqueous Solutions. The aggregation behavior of **1-F** was studied in aqueous solutions containing THF as a cosolvent. The choice of THF was based on its ability to dissolve PDI derivatives and its good miscibility with water. Thus, THF was used to attenuate the hydrophobic effect, crucial for structural and thermodynamic investigations under equilibrium conditions. In dilute THF solution (10^{-5} M), **1-F** shows strong fluorescence and UV/vis absorption bands, characteristic of fully disaggregated PDI (Figure 2, Figure S12). Increasing volume fractions of water cause distinct spectral changes and strongly quench the molecules' fluorescence. The absorbance changes include peak broadening and changes in the relative intensity of the 0-0 and 0-1 vibronic transitions as well as an overall hypsochromic shift (Figure 2, Figure S35). These changes are characteristic of PDI H-aggregates, indicating that face-to-face stacking with small longitudinal displacement is the dominating stacking geometry.[36,37] The same spectral changes were observed in **1-H** (Figure S13), suggesting that its stacking geometry is very similar to that of **1-F**. These changes are analogous to previously reported columnar stacks of PDI H-aggregates in aqueous medium.[29]

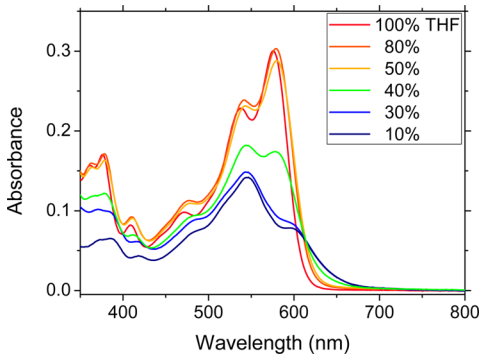

Figure 2. UV/vis spectra of **1-F** (10^{-5} M) in water/THF mixtures. Decreasing THF volume fractions result in distinct spectral changes, indicating H-aggregation.

Figure 3 shows the proposed stacking geometry of the dimer of **1-F** obtained from optimization by the semiempirical PM6-DH+ method[42] together with COSMO[41] model for solvent approximation (see Supporting Information). An analogous dimer structure is proposed for compound **1-H** (Figure S14). This method accounts for noncovalent interactions, but it omits specific solvophobic effects. Yet, the close packing of nonpolar groups in the models is expected to be favored by the hydrophobic effect. In the proposed dimer structures, the PDI groups are closely stacked face to face, exhibiting a typical stacking distance of 3.5 Å. Moreover, there is a significant rotational displacement of 24°, which is similar to values in some other π-stacked *N*-alkyl-PDIs (e.g., ~30°).[29,43] The relative intermolecular orientation corresponds to H-aggregated PDI, which is supported by the observed changes in the absorption spectra (Figure 2, Figure S35). The molecular model also reveals the presence of an H-bond (2.0 Å H−O distance) between amide groups. Overall, the proposed dimer models of both compounds are in good agreement with the observed UV/vis spectra and can be used to model supramolecular fiber structures formed by both compounds in water/THF mixtures, resulting in good fits to the fiber structures observed by cryo-TEM (see below).

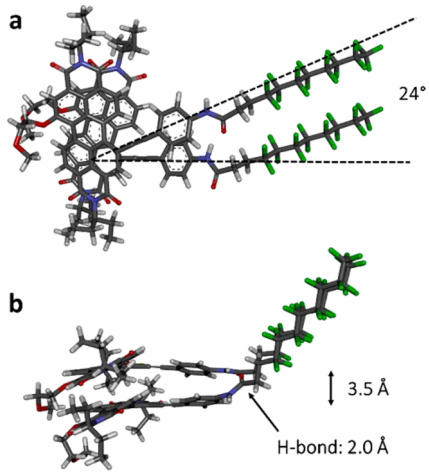

Figure 3. Proposed stacking geometry in the **1-F** dimer. (a) View perpendicular to the aromatic surface (b) View parallel to the aromatic surface.

Structural Study by Electron Microscopy. Structural investigation of the supramolecular morphologies was performed by electron microscopy. Cryogenic transmission electron microscopy (cryo-TEM) images of **1-F** in water/THF mixture with high THF volume fraction (35%) show thin and uniform fibrous aggregates (Figure 4a). The fibers tend to locally align with ~8.2 nm interfiber spacings, as revealed by analysis using fast Fourier transform (FFT, Figure 4a, inset). The observed spacing corresponds to the sum of the directly measured high-contrast fiber core (2.8 ± 0.7 nm) and the low-contrast PEG shell (5.5 ± 0.5 nm), and it matches previously reported spacings between fibers of PEG−PDI amphiphiles.[25,26] TEM images of dried samples show identical fibers with diameters of 2.7 ± 0.6 nm (Figure S15).

As opposed to **1-F**, non-fluorinated**1-H** assembles under the same conditions into much smaller aggregates having very low contrast (Figure S16). They exhibit average spacings of ~7.6 nm (from FFT) in 65:35 water/THF (v/v), similar to those observed for **1-F**. Even in solutions with significantly higher water contents (80:20 water/THF (v/v)), **1-H** assembled into rather short fibers that were up to several tens of nanometers in length (Figure 4b). The fibers were 2.0 ± 0.3 nm wide and separated by spacings of ~7.5 nm (from FFT), which are virtually identical to those observed at lower water content.

The relatively small diameters of the observed fibers of **1-F** and **1-H** imply a simple supramolecular architecture with linearly π-stacked PDI groups. Figure 4c shows proposed

dx.doi.org/10.1021/ja503906p | J. Am. Chem. Soc. 2014, 136, 9443−9452

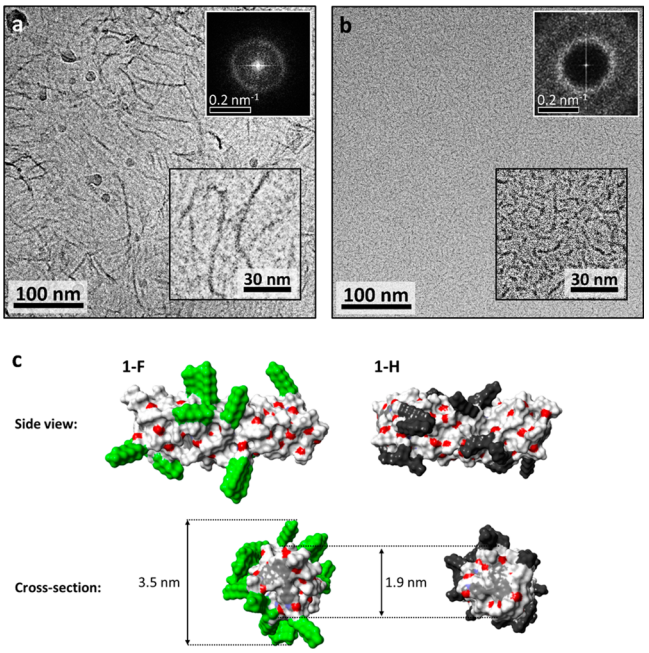

Figure 4. Supramolecular polymer fibers of **1-F** and **1-H**. (a) Cryo-TEM image of **1-F** (10^{-4} M) in 65:35 water/THF (v/v). The fibers have high-contrast cores with diameters of 2.8 ± 0.7 nm and lengths in the order of ~100 nm. Spherical objects are ice crystals that formed during sample preparation. Inset: FFT of the image, revealing a periodicity of ~8.2 nm, which corresponds to the average fiber−fiber spacing. (b) Short supramolecular fibers of **1-H** (10^{-4} M) in 80:20 water/THF (v/v). Lower inset: High-magnification image revealing fibers with 2.0 ± 0.3 nm diameter high-contrast cores and lengths of up to several tens of nanometers. Upper inset: FFT calculation of the image, revealing a periodicity of 7.5 nm, which corresponds to the average fiber−fiber distance. (c) Proposed molecular models of the supramolecular fibers of **1-F** and **1-H**. The geometries were obtained by molecular dynamics simulations and subsequent molecular mechanics optimization (see Supporting Information). The models show the solvent-accessible surface area. Perfluorooctyl groups in **1-F** are shown in green; the nonfluorinated alkyl chains in **1-H** are shown in black. For simplification, PEG chains were modeled as $-O(CH_2-CH_2)OCH_3$ groups.

molecular models of the fibers composed of **1-F** and **1-H**. The models were constructed to fit best the cryo-TEM data. They exhibit a columnar fiber propagation, where the uniform columnar assembly is based on the stacking geometry in the dimers (Figure 3, Figure S14). The final geometry was obtained after a molecular dynamics equilibration and subsequent molecular mechanics energy minimization (see Supporting Information). The densely stacked fiber cores in both models are 1.9 nm thick, corresponding to the observed diameter of fibers of **1-H** (2.0 ± 0.3 nm). The average diameter of **1-F** fibers is somewhat larger (2.8 ± 0.7 nm) than in **1-H**, which can be explained by the protruding F-chains. The average interfiber distance in both systems is very similar. The observed fiber diameter of **1-F** lies in between the value for the modeled fiber core (1.9 nm) and the maximum diameter of the extended fluorocarbon chains (3.5 nm, Figure 4c).

The difference between the proposed models of **1-F**- and **1-H**-based fibers owes to the conformation of the fluorinated vs non-fluorinated alkyl chains. The hydrocarbon chains in fibers of **1-H** readily attain both gauche and anti conformations, which allows them to turn back and interact with the hydrophobic fiber surface, thus minimizing contact with the aqueous environment. In contrast, the fluorocarbon chains in the proposed model of **1-F** have a rigid all-trans conformation, which is in agreement with reported crystal structural data of perfluoroalkyl chains.[31] Thus, the fluoroalkyl chains in **1-F** are extended and point away from the hydrophobic fiber core, resulting in a large contact surface with the surrounding medium. This difference is also supported by the observed differences in fiber width (Figure 4a,b). Although contacts between neighboring fluorocarbon chains reduce this interface, the exposure of an extended fluorocarbon surface should be energetically unfavorable in an aqueous environment. Significant amounts of THF (35% v/v) may aid in solvation of these hydrophobic moieties. Moreover, the long PEG chains surrounding the supramolecular fiber (depicted in Figure S19) envelop the fluoroalkyl groups, thus reducing the interface with the polar medium. The difference in conformational flexibility of the fluoroalkyl vs alkyl chains appears to have a profound impact on the aggregation thermodynamics and mechanism (see below).

Increasing volume fractions of water (≥70%) in solutions of **1-F** cause a morphological transformation, affording fibers with diameters of 5−6 nm. It was possible to resolve the fine structure of these fibers having tube-like morphology (Figure 5). In 70:30 water/THF (v/v) these structures were 5.3 ± 0.8 nm in diameter and 36 ± 16 nm in length (Figure 5a). In 80:20 water/THF (v/v) the fibers exhibit lengths up to several micrometers, while retaining their average diameter (5.8 ± 0.8 nm, Figure 5b,c). The high aspect ratio fibers were occasionally

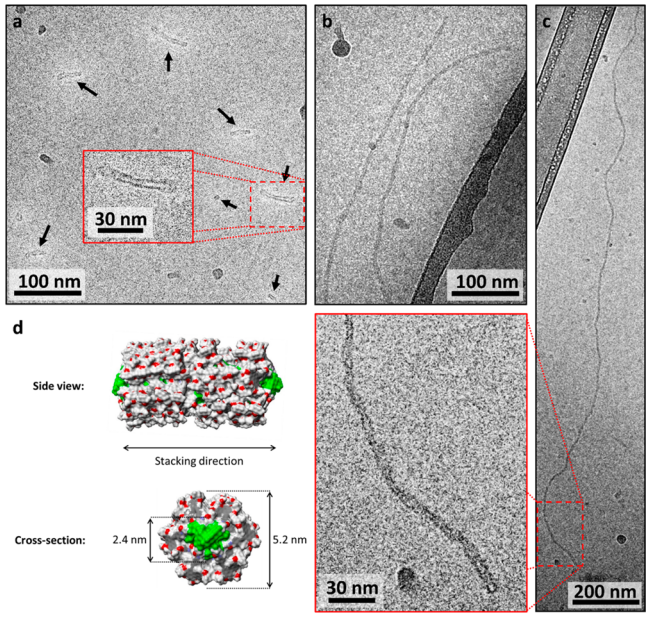

Figure 5. Cryo-TEM images of **1-F** tube-like fibers. (a) **1-F** (10^{-4} M) in 70:30 water/THF (v/v) showing short tube-like fibers 5.3 ± 0.8 nm in diameter and 36 ± 16 nm in length (black arrows). (b,c) **1-F** (10^{-4} M) in 80:20 water/THF (v/v) showing long tube-like fibers with diameters of 5.8 ± 0.8 nm and micrometer-scale lengths. Zoom-in: High-magnification image of a nanofiber and its end-cap, revealing its tubular morphology and small variations in fiber diameter. (d) Proposed molecular model. The geometry was obtained by molecular mechanics optimization following molecular dynamics equilibration. The model shows the solvent-accessible surface area. Perfluorooctyl groups are shown in green. For simplification, PEG chains were modeled as $-O(CH_2-CH_2)OCH_3$ groups.

dx.doi.org/10.1021/ja503906p | J. Am. Chem. Soc. 2014, 136, 9443−9452

bundled to form larger structures (Figure S17), and extended fiber bundles were observed in TEM images after drying (Figure S18). The morphology can be modeled as a tube-like fiber, where an inner compartment of randomly oriented perfluorooctyl chains is surrounded by a ring of PDI groups that undergo π-stacking in the direction of fiber propagation (Figure 5d). Thermally equilibrated (crystalline) fluorous domains give usually strong contrast in cryo-TEM, whereas less ordered domains result in lower contrast.[44] Thus, relatively low contrast of the inner fiber compartment (Figure 5) suggests that the fluorous core is less ordered than the fiber wall, constructed from densely π-stacked PDI groups. Such fiber morphology requires a diameter of at least ~5.2 nm, which is in good agreement with the observed fiber diameters.

Greater water contents in solutions of **1-F** further increased the driving force of aggregation, and the system was observed to form a gel in 90:10 water/THF (v/v) above a critical concentration of ~6×10^{-3} M (1.1 wt%) (Figure 6a).

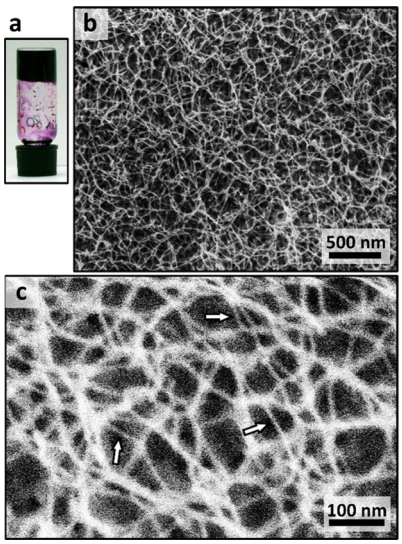

Figure 6. 1-F in water/THF (90:10, v/v). (a) Image of an inverted vial containing the gelled material (6×10^{-3} M). (b) Cryo-SEM image of a viscous solution of **1-F** (5.6×10^{-3} M) showing an extended three-dimensional fibrous network. (c) Higher magnification image revealing individual fibers (marked by white arrows) along with fiber bundles. The widths of the highlighted fibers are 6–7 nm.

Interestingly, gelation took place only after the sample solution had been heated in a sealed vial at 50 °C for 30 min, after which it remained solid at room temperature. This irreversible behavior appears to be a result of PEG desolvation followed by fiber entanglement.[26] In order to characterize the supramolecular structure of this highly concentrated and viscous system, we employed cryogenic scanning electron microscopy (cryo-SEM). Cryo-SEM images showed extended supramolecular fibers and fiber bundles (Figure 6b,c). While the cryogenic methodology is designed to minimize formation of ice crystals, the spacings between the fibers might be somewhat changed due to devitrification (see Supporting Information), while the fiber structure should be retained. The thinnest individual fibers were 6–7 nm wide, in good agreement with the modeled structure having 5.2 nm hydrophobic core surrounded by a shell of collapsed (dehydrated) PEG.

Overall, the fibers of **1-F** are at least 2 orders of magnitude longer than the linear stacks observed for **1-H** under the same conditions. The large differences in the degree of supramolecular polymerization implies a large difference in thermodynamic driving force for aggregation. Moreover, while linear aggregates of **1-H** grow with increasing water content, they show no sign of morphology change (see Figure 4b and Figure S16). In contrast, fibers of **1-F** undergo a morphology transformation between 30 and 35% THF, which suggests a change in aggregation mechanism.

Cooperativity and Aggregation Mechanism. In order to assess the strength of noncovalent binding in **1-F** as compared to **1-H**, and to elucidate the mechanism of self-assembly, we complemented our microscopic imaging with thermodynamic studies, employing temperature-dependent UV/vis spectroscopy at different concentrations and THF volume fractions.[45] Due to the strength of hydrophobic forces acting on **1-F**, aqueous solutions with less than 25% THF content showed no temperature- or concentration-dependent disaggregation. Yet, higher volume fractions of THF sufficiently attenuate the hydrophobic effect, enabling temperature-dependent aggregation/disaggregation. The absorption spectra of **1-F** (10^{-5} M) in 65:35 water/THF (v/v) at different temperatures are presented in Figure 7a. The spectral changes are identical to those caused by changing THF contents (see Figure 2). At high temperature (65 °C) the molecules are disassembled, whereas at lower temperatures (<35 °C) almost all molecules are in an aggregated state. The clear isosbestic point at 609 nm indicates that there is only one spectroscopically discernible type of aggregates (i.e., H-aggregates) besides the monomer species. The spectral changes enable determination of the degree of aggregation, α, which is the fraction of molecules in the aggregated state.[6] Notably, for **1-F**, the temperature dependence of α reveals an asymmetric sigmoid curve that does not fit the simple isodesmic aggregation model (Figure 7b).[6] The sharp onset of aggregation upon cooling indicates cooperative self-assembly, which implies a nucleation and chain elongation mechanism.[8] Indeed, the cooperative model for *thermally activated equilibrium polymers* that was developed by van der Schoot, Meijer, and co-workers[6,8,46,47] is in excellent agreement with the data (red trace in Figure 7b). The curve fitting yielded important parameters of the self-assembly, including the enthalpy of the noncovalent bonds at the critical temperature of polymerization onset, T_e (ΔH_e = −86 ± 11 kJ/mol), the dimensionless equilibrium constant of the activation step at T_e ($K_a \approx 3 \times 10^{-3}$, indicating a high degree of cooperativity), and the average number of molecules in an aggregate at that temperature, $\langle N(T_e)\rangle$. The latter gives an estimate of the size of the nucleating aggregate. Due to the expected difference in hydrophobicity, **1-H** requires higher concentrations to achieve the same degree of aggregation. Unlike its fluorinated counterpart, **1-H** shows aggregation curves that are in good agreement with the isodesmic model[6,46] (Figure 7c). We note that the interactions between the fluoroalkyl and alkyl groups in the assemblies do not give rise to typical signals in UV/vis spectra, yet they contribute to the observed aggregation behavior. Their contribution is accounted for in the overall thermodynamic analysis since in the studied equilibrating systems, PDI cores (very large hydrophobic/stacking moieties) show reversible H-aggregation (probed by UV/vis), coexisting with the interactions between the alkyl and fluoroalkyl groups (evident from the structural analysis of the fibers). It should be noted that in the equilibrating systems under study we cannot detect the sequence of interaction

dx.doi.org/10.1021/ja503906p | J. Am. Chem. Soc. 2014, 136, 9443–9452

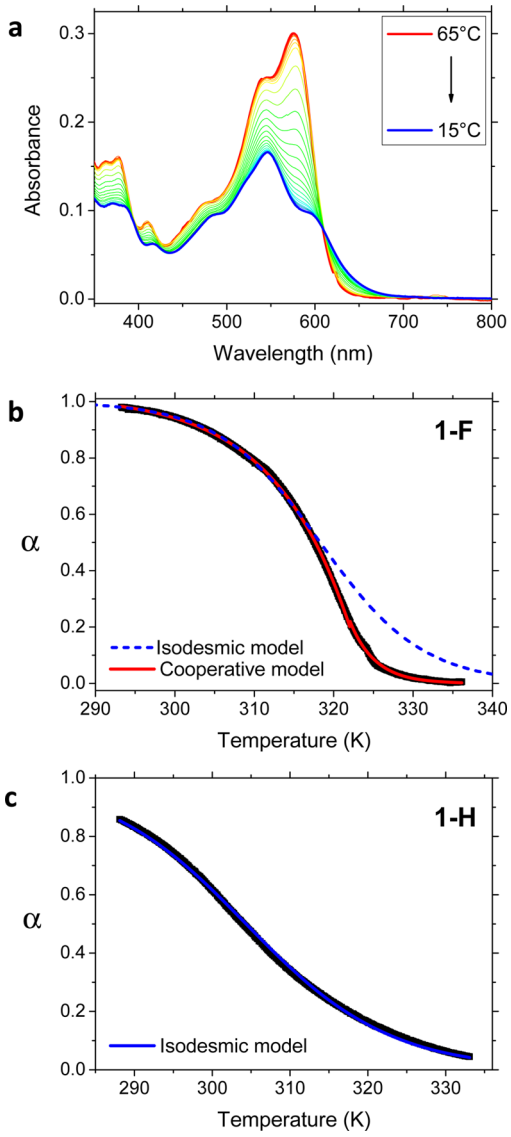

Figure 7. Temperature-dependent aggregation study in water/THF (65:35, v/v). (a) UV/vis absorption spectra of **1-F** (10^{-5} M). (b) Degree of aggregation, α, as a function of temperature (black data points) for **1-F** (10^{-5} M), fitted by the cooperative model (red line), as compared to the isodesmic model (blue dashed line). (c) α vs temperature (black data points) for **1-H** (5.7×10^{-5} M) and isodesmic fit (blue line).

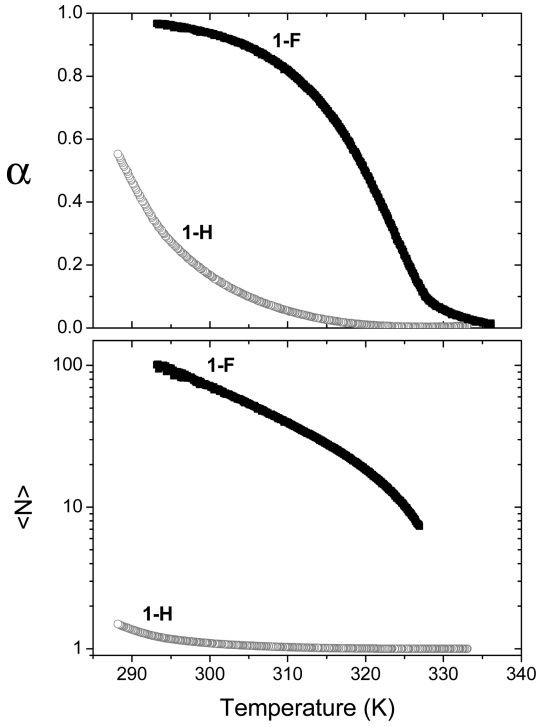

Figure 8. Aggregation behavior of **1-F** and **1-H** under the same conditions (10^{-5} M, 65:35 water/THF (v/v)). Top: temperature dependence of the degree of aggregation, α. Bottom: Calculated number-averaged degree of polymerization in the elongation regime (averaged over all active species) of **1-F**, and number-averaged aggregate size of **1-H**.

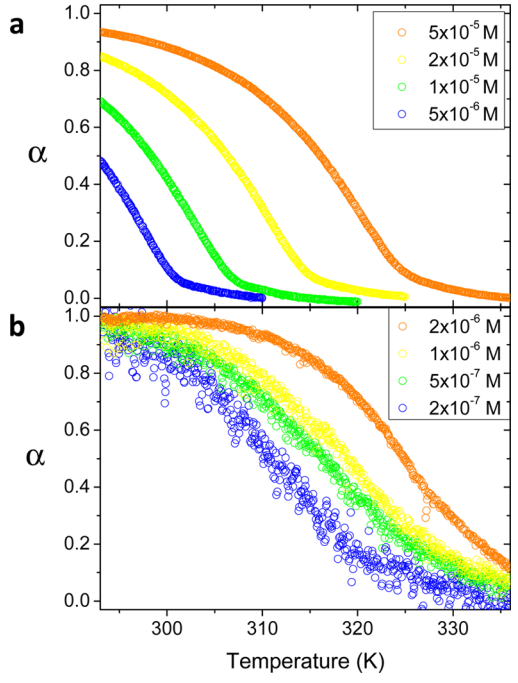

Figure 9. Aggregation curves for **1-F** in different water/THF mixtures (v/v): (a) 60:40 and (b) 70:30.

events. The related kinetic studies are beyond the scope of this work, and represent a subject of ongoing studies.

Figure 8 illustrates the combined effect of cooperativity and aggregation strength of **1-F** as compared to **1-H** under the same conditions. The larger value of α in **1-F** is mostly a result of its stronger free energy of aggregation (see below), whereas the very large difference in the number-averaged aggregate size, $\langle N \rangle$, is a combined effect of strong binding and cooperativity. At room temperature, stacking lengths in **1-F** are 2 orders of magnitude larger than in **1-H**, which is in excellent agreement with the structural differences observed in cryo-TEM (see Figure 4a vs Figure S16).

Surprisingly, the strong cooperativity of **1-F** aggregation observed in aqueous solutions with high THF content (≥35%) is lost in solutions with lower THF content, resulting in ideal isodesmic aggregation (Figure 9). This sudden change in cooperativity parallels the morphological transformation observed by cryo-TEM: the cooperative growth in high THF content solutions produces helical columnar stacks, whereas isodesmic aggregation leads to the formation of tube-like structures. Figure 10 displays the change in cooperativity and

dx.doi.org/10.1021/ja503906p | J. Am. Chem. Soc. 2014, 136, 9443−9452

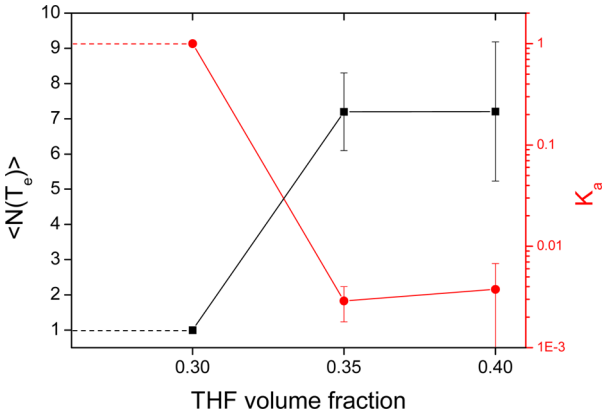

Figure 10. Cooperativity switching of **1-F**. Dependence of the calculated size of the nucleus ($\langle N(T_e)\rangle$, black data points) and the corresponding dimensionless equilibrium constant of the activation step (K_a, red data points) on the THF content.

nucleus size around the crossover region between cooperative and isodesmic aggregation of **1-F**. The calculated size of the aggregation nucleus in 65:35 and in 60:40 water/THF (v/v) solutions is identical within experimental error (7.2 ± 1.1 and 7.2 ± 2.0 molecules, respectively).

The observed aggregation characteristics are remarkable: (1) In the presence of large THF volume fractions **1-F** exhibits cooperative aggregation. However, cooperativity is not observed in reference compound **1-H**, despite its very similar molecular and supramolecular structure. (2) **1-F** aggregation becomes isodesmic in solutions with lower THF content, resulting in morphological transformation from helical molecular stacks to tube-like fibers.

Detailed understanding of cooperative mechanisms is rare,[7,47−49] but previous studies have shown that cooperativity effects can be a result of helicity.[7,11,47,48] While molecular modeling and dynamics simulations are inherently limited for large supramolecular systems, our studies offer tentative explanations for both cooperativity and structure switching, which are in good agreement with the experiments. The calculated size of the nucleus of **1-F** polymerization (∼7.2) corresponds well to a half helical turn of the modeled fiber (180°/24° [rotational displacement in the lowest energy dimer model] = 7.5). As discussed above, formation of helical columnar stacks from **1-F** would expose the rigid fluorocarbon chains to the aqueous environment. The PEG groups comprising the fiber shell can act as a stabilizer, but in molecular stacks shorter than a half-helical turn, such stabilization is hampered, since PEG groups and fluoroalkyl groups lie on opposite sides of the forming fiber (Figure 11; a molecular model including PEG chains is shown in Figure S19). This effect is not pronounced in **1-H**, as the alkyl groups are flexible, leading to close contacts with the hydrophobic fiber surface. Thus, the cooperativity of aggregation in the presence of fluoroalkyl chains could arise due to the helicity of the supramolecular fiber together with the conformational rigidity of the sterically demanding fluorocarbon chain. We note that the sequence of interaction events presented in Figure 11 is tentative and will need to be addressed via kinetic studies.

The idea that cooperativity of **1-F** aggregation is a result of the helicity may explain why aggregation becomes non-cooperative in solutions with high water content, where non-helical tubular fibers are observed. Here, the hydrophobic interactions become stronger, imposing F-chains' encapsulation in the inner fiber compartment, similarly to microphase separations observed in fluorinated block copolymer systems.[50]

Tables 1 and 2 summarize the thermodynamic parameters of **1-F** and **1-H** supramolecular polymerization, as determined by curve fitting and van't Hoff analysis (see Supporting Information). Enthalpies obtained via van't Hoff analysis were in good agreement with those obtained from curve fitting, indicating consistency of the thermodynamic data. The latter reveals that for both compounds the aggregation process is enthalpically driven and entropically disfavored in the tested window of THF volume fractions (cf. Figure S33). The strong enthalpic driving force is an example of the "nonclassical" hydrophobic effect,[51] which can be attributed to (1) the large nonpolar surfaces that break the attractive interactions within the 3D hydrogen bonding network of water[24] and (2) attractive $\pi-\pi$ interactions and H-bonding between the assembling molecules.

Expectedly, the value of ΔG° (the Gibbs free energy of association at 298 K) strongly increases with increasing water content. Thus, the values of the association constants steeply grow with decreasing THF content, reaching the highest directly measurable value of 1.7×10^9 M^{-1} for **1-F** in 75:25 water/THF (v/v). In the same solvent mixture the association constant for **1-H** was 8.8×10^6 M^{-1}. Neither **1-F** nor **1-H** could be disaggregated in solutions with low THF content. For example, **1-F** remained fully aggregated at concentrations of 5×10^{-7} M in 99:1 water/THF (v/v) and at 5×10^{-9} M in 95:5 water/THF (v/v), even when the solution was heated to the boiling point (Figure S23).

The high noncovalent stability precludes direct determination of ΔG° values in neat water. As shown in Figure 12, ΔG° of **1-H** and **1-F** exhibits an approximately linear dependence on the THF content within the experimentally accessible window of solvent mixtures (20−40 vol% THF). Analogous to a common method for the study of protein folding,[52] the linear trend of ΔG° was extrapolated, in order to assess the noncovalent binding strength of **1-F** and **1-H** in pure water (Figure 12).

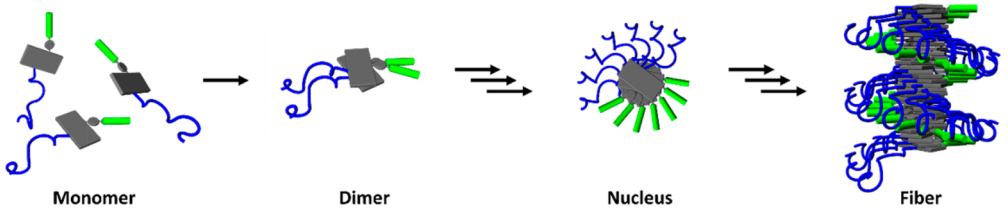

Figure 11. Schematic illustration of the proposed mechanism of the cooperative aggregation of **1-F**. In aggregates larger than the critical nucleus size, PEG groups (blue) can envelope F-chains (green), thus reducing unfavorable interactions of the latter with the aqueous environment.

dx.doi.org/10.1021/ja503906p | J. Am. Chem. Soc. 2014, 136, 9443−9452

Table 1. Thermodynamic Parameters of 1-F Supramolecular Polymerization in Different Water/THF Mixtures

THF vol%	ΔH (kJ/mol)[a]	$\Delta H°$ (kJ/mol)[b]	$-T\Delta S°$ (kJ/mol)[b]	$\Delta G°$ (kJ/mol)[b]	K (M^{-1})[b]
25	−118.8 ± 1.5	−115.4 ± 2.4	62.7 ± 2.2	−52.7 ± 3.3	1.7×10^9
30	−148 ± 17	−144 ± 16	101 ± 14	−42.8 ± 1.4	3.7×10^7
35	−86 ± 11	−84.5 ± 4.3	48.6 ± 4.1	−35.9 ± 5.9	1.9×10^6
40	−72.2 ± 7.7	−79.9 ± 1.9	49.0 ± 1.9	−30.9 ± 2.7	2.6×10^5

[a]Obtained from curve fitting. Values refer to the critical temperature of melting/elongation. [b]Obtained from van't Hoff analysis. Values refer to 298 K.

Table 2. Thermodynamic Parameters of 1-H Supramolecular Polymerization in Different Water/THF Mixtures

THF vol%	ΔH (kJ/mol)[a]	$\Delta H°$ (kJ/mol)[b]	$-T\Delta S°$ (kJ/mol)[b]	$\Delta G°$ (kJ/mol)[b]	K (M^{-1})[b]
20	−78 ± 16	−62 ± 11	19 ± 10	−43.6 ± 0.7	4.4×10^7
25	−112 ± 32	−106 ± 27	67 ± 26	−39.2 ± 1.8	8.8×10^6
30	−122 ± 22	−133 ± 13	101 ± 13	−32.5 ± 0.6	5.0×10^5
35	−98 ± 8	−92.0 ± 0.2	67.2 ± 0.2	−24.8 ± 0.2	2.2×10^4

[a]Obtained from curve fitting. Values refer to the critical temperature of melting. [b]Obtained from van't Hoff analysis. Values refer to 298 K.

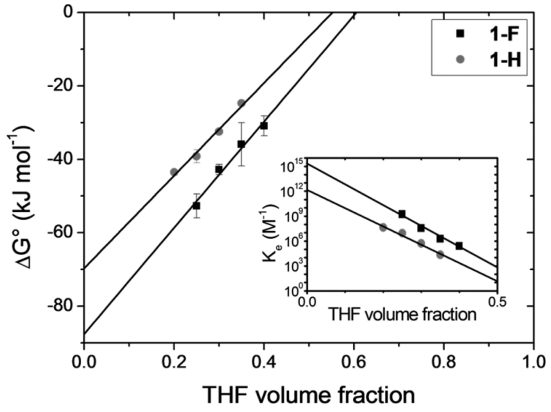

Figure 12. Strength of noncovalent bonding of **1-F** and **1-H** in aqueous solutions with different THF volume fraction. Measured values of $\Delta G°$ and regression lines. Inset: corresponding equilibrium constants.

In protein folding studies, extrapolation of thermodynamic parameters typically yields a *lower estimate* of the thermodynamic driving force.[52] A linear free energy relationship has been previously assumed in the study of self-assembling dye molecules.[53] Recent findings by Würthner and co-workers show that the driving force of PDI self-assembly is linearly dependent on the empirical solvent polarity parameter $E_T(30)$,[54,55] which itself is a function of THF content.[56] Their study also showed that in neat water the strength of aggregation is in fact *underestimated* by this linear free energy relationship. Whereas the value of $E_T(30)$ itself shows good linear dependence on THF content between 20 and 80 vol%, it becomes significantly larger than expected for pure water (Figure S34). The above-described findings indicate that linear extrapolation of $\Delta G°$ of **1-H** and **1-F** will yield a *lower limit estimate* of the driving force of aggregation in neat water. Based on our extrapolation, the lower estimate of the Gibbs free energy of **1-F** aggregation in pure water is −87.0 ± 5.1 kJ/mol, corresponding to an equilibrium constant for noncovalent chain elongation of $K \approx 2 \times 10^{15}$ M^{-1} (inset in Figure 12). To the best of our knowledge, this value is larger than that in any other noncovalent polymer; it is also larger than reported values for most coordination polymers.[57,58]

We note that a potentially important requirement for extrapolation of aggregation thermodynamics is that the molecular packing within the aggregates is not altered by the different solvent environments. The morphological and mechanistic changes of **1-F** polymerization (see above) appear to have slight impact on the linear trend of $\Delta G°$. The small degree of nonlinearity can be explained by the fact that interaction patterns (H-stacks and interactions between other hydrophobic moieties) are similar over the range of water/THF ratio (as revealed by UV/vis spectroscopy, cf. Figure 2, Figure S35). Evidently, the deviation from linearity should be toward more negative $\Delta G°$ values, due to somewhat larger overlap of hydrophobic surfaces upon structural switching in **1-F**. We note that at THF content as low as 10%, the fiber motif is preserved (Figure 6). While the extrapolated estimate of hydrophobic interactions is approximate, it gives the *lower limit for hydrophobic interactions*, as the latter were observed to be stronger than estimated by various indirect methods.[56] Such estimate is important since it provides a semiquantitative measure to asses a potential of hydrophobic interactions for creating robust noncovalent systems.

There is a significant difference in the estimated binding strength between the two analogues (17.8 ± 5.9 kJ/mol). Is this difference a result of a unique nature of fluorocarbon hydrophobicity, or merely an effect of the different size of molecular surfaces in **1-F** vs **1-H** (ΔSAS = 87 Å^2; ΔSES = 68 Å^2)? In order to address this question, we compared the experimentally observed difference in $\Delta G°$ to values that would be expected for non-fluorinated alkanes. Two empirical relationships between $\Delta G°$ and the hydrophobic surface of alkyl chains have been reported: (1) $\Delta G°$ is linearly dependent on incremental changes in the SAS. Depending on the assumptions made, the relationship is given by a value between 84 and 138 J mol^{-1} Å^{-2}.[22] (2) Instead of using the SAS, it was suggested that $\Delta G°$ is proportional to the SES, where the proportionality constant of 290 J mol^{-1} Å^{-2} is very close to the macroscopic oil/water interfacial energy (~310 J mol^{-1} Å^{-2}).[23] Disregarding the controversy[59,60] about which of these two approaches accurately reflects the strength of the hydrophobic effect, we compared the predicted free energy differences derived from both methods with the experimental one. The former approach predicts a value of 7.3−12.0 kJ/mol, whereas the latter gives a value of 20.4 kJ/mol. Our experimental value of 17.8 ± 5.9 kJ/mol lies in between these estimates. Therefore, rather than presuming a unique nature of fluorocarbon hydrophobicity, the large driving force of **1-F** aggregation can

dx.doi.org/10.1021/ja503906p | J. Am. Chem. Soc. 2014, 136, 9443−9452

be attributed to the bulkiness and, hence, larger hydrophobic surface of the fluorocarbon chain as compared to its non-fluorinated counterpart. This interpretation agrees with theoretical studies[34] and with experimental reports comparing fluorocarbon and hydrocarbon binding to nonpolar cavities.[35]

We note that the dependence of the hydrophobic driving force on the size of nonpolar surface area implies that ultrastrong noncovalent binding could be generally achieved in many alternative amphiphilic systems. For instance, several supramolecular polymers that were previously reported by our group[25−27] may exhibit similar or even stronger noncovalent binding in aqueous media, as compared to compound **1-F**, when one considers the large hydrophobic surfaces employed to assemble these systems. While being strong in pure water, the hydrophobic interactions can be attenuated via addition of organic cosolvent to result in dynamic behavior, enabling tunable bonding strength, reversibility, and structure switching.[25−27]

CONCLUSIONS

Compound **1-F** combines $\pi-\pi$/hydrophobic interactions of the PDI unit, H-bonding, and fluorocarbon hydrophobicity to form an exceptionally stable, homogeneously dissolved supramolecular polymer. The polymer fibers of **1-F** were 2 orders of magnitude longer than in the case of non-fluorinated analogue **1-H** under the same conditions, and association constants were up to 3 orders of magnitude larger. In pure water, the association constant of **1-F** was estimated by extrapolation to be at least in the order of 10^{15} M^{-1}. Under these conditions, fiber disassembly cannot be achieved, even at very low concentrations and temperatures close to the boiling point. Such strong binding is advantageous for the development of highly robust, mechanically stable noncovalent nanomaterials, which will exhibit negligible leaching of monomer units into the environment. Yet, in the presence of sufficient organic cosolvent (25−40% THF, v/v), the polymer retains its adaptive properties, allowing for dynamic assembly/disassembly.

Changes in THF content alter the aggregation mechanism of **1-F**, accompanied by a morphological transformation: cooperatively aggregating columnar stacks are observed in the presence of large THF volume fractions, whereas smaller amounts of organic cosolvent cause isodesmic formation of tube-like fibers.

The large hydrophobic driving force of **1-F** polymerization can be explained on the basis of the large surface of the F-chain. However, the cooperative polymerization mechanism appears to be a specific result of F-chain conformational rigidity, shedding light on the factors governing fluorocarbon self-assembly in aqueous medium. The distinctive properties of fluorocarbon groups provide a promising tool for noncovalent polymer synthesis, enabling exceptional stability, control over morphology, and switchable self-assembly mechanism. Our future studies will aim at investigating materials based on the **1-F** supramolecular polymer.

ASSOCIATED CONTENT

Supporting Information

Experimental details of synthesis and characterizations of compounds **1-H** and **1-F**; additional experimental procedures, electron microscopic images, spectroscopic data, and thermodynamic analysis. This material is available free of charge via the Internet at http://pubs.acs.org.

AUTHOR INFORMATION

Corresponding Author

boris.rybtchinski@weizmann.ac.il

Notes

The authors declare no competing financial interest.

ACKNOWLEDGMENTS

This work was supported by grants from the Israel Science Foundation, Minerva Foundation, KAMIN program administered by the Israel Ministry of Economy, the Schmidt Minerva Center for Supramolecular Architectures, and the Helen and Martin Kimmel Center for Molecular Design. The EM studies were conducted at the Irving and Cherna Moskowitz Center for Nano and Bio-Nano Imaging (Weizmann Institute). The authors thank Samuel A. Safran, Maya Bar-Sadan, and Sharon G. Wolf for valuable discussions, and David Margulies for permission to use instruments in his laboratories.

REFERENCES

(1) Ciferri, A. *Supramolecular Polymers*, 2nd ed.; CRC Press: Boca Raton, FL, 2005.
(2) De Greef, T. F. A.; Smulders, M. M. J.; Wolffs, M.; Schenning, A. P. H. J.; Sijbesma, R. P.; Meijer, E. W. *Chem. Rev.* **2009**, *109*, 5687−5754.
(3) Aida, T.; Meijer, E. W.; Stupp, S. I. *Science* **2012**, *335*, 813−817.
(4) Yan, X.; Wang, F.; Zheng, B.; Huang, F. *Chem. Soc. Rev.* **2012**, *41*, 6042−6065.
(5) Bosman, A. W.; Sijbesma, R. P.; Meijer, E. W. *Mater. Today* **2004**, *7*, 34−39.
(6) Smulders, M. M. J.; Nieuwenhuizen, M. M. L.; de Greef, T. F. A.; van der Schoot, P.; Schenning, A. P. H. J.; Meijer, E. W. *Chem.—Eur. J.* **2010**, *16*, 362−367.
(7) Zhao, D.; Moore, J. S. *Org. Biomol. Chem.* **2003**, *1*, 3471−3491.
(8) Jonkheijm, P.; van der Schoot, P.; Schenning, A. P. H. J.; Meijer, E. W. *Science* **2006**, *313*, 80−83.
(9) Sijbesma, R. P.; Beijer, F. H.; Brunsveld, L.; Folmer, B. J. B.; Hirschberg, J. H. K. K.; Lange, R. F. M.; Lowe, J. K. L.; Meijer, E. W. *Science* **1997**, *278*, 1601−1604.
(10) Söntjens, S. H. M.; Sijbesma, R. P.; van Genderen, M. H. P.; Meijer, E. W. *J. Am. Chem. Soc.* **2000**, *122*, 7487−7493.
(11) Jin, W.; Fukushima, T.; Niki, M.; Kosaka, A.; Ishii, N.; Aida, T. *Proc. Natl. Acad. Sci. U.S.A.* **2005**, *102*, 10801−10806.
(12) Zhang, W.; Jin, W.; Fukushima, T.; Ishii, N.; Aida, T. *J. Am. Chem. Soc.* **2013**, *135*, 114−117.
(13) Chen, Z.; Lohr, A.; Saha-Moller, C. R.; Würthner, F. *Chem. Soc. Rev.* **2009**, *38*, 564−584.
(14) Schmuck, C.; Wienand, W. *J. Am. Chem. Soc.* **2002**, *125*, 452−459.
(15) Gröger, G.; Meyer-Zaika, W.; Böttcher, C.; Gröhn, F.; Ruthard, C.; Schmuck, C. *J. Am. Chem. Soc.* **2011**, *133*, 8961−8971.
(16) Holyer, R. H.; Hubbard, C. D.; Kettle, S. F. A.; Wilkins, R. G. *Inorg. Chem.* **1966**, *5*, 622−625.
(17) Oshovsky, G.; Reinhoudt, D.; Verboom, W. *Angew. Chem., Int. Ed.* **2007**, *46*, 2366−2393.
(18) Krieg, E.; Rybtchinski, B. *Chem.—Eur. J.* **2011**, *17*, 9016−9026.
(19) Hartgerink, J. D.; Beniash, E.; Stupp, S. I. *Proc. Natl. Acad. Sci. U.S.A.* **2002**, *99*, 5133−5138.
(20) Obert, E.; Bellot, M.; Bouteiller, L.; Andrioletti, F.; Lehen-Ferrenbach, C.; Boué, F. *J. Am. Chem. Soc.* **2007**, *129*, 15601−15605.
(21) Ball, P. *Chem. Rev.* **2008**, *108*, 74−108.
(22) Tanford, C. *Proc. Natl. Acad. Sci. U.S.A.* **1979**, *76*, 4175−4176.
(23) Tuñón, I.; Silla, E.; Pascual-Ahuir, J. L. *Protein Eng.* **1992**, *5*, 715−716.
(24) Chandler, D. *Nature* **2005**, *437*, 640−647.

(25) Baram, J.; Shirman, E.; Ben-Shitrit, N.; Ustinov, A.; Weissman, H.; Pinkas, I.; Wolf, S. G.; Rybtchinski, B. *J. Am. Chem. Soc.* **2008**, *130*, 14966−14967.
(26) Krieg, E.; Shirman, E.; Weissman, H.; Shimoni, E.; Wolf, S. G.; Pinkas, I.; Rybtchinski, B. *J. Am. Chem. Soc.* **2009**, *131*, 14365−14373.
(27) Ustinov, A.; Weissman, H.; Shirman, E.; Pinkas, I.; Zuo, X.; Rybtchinski, B. *J. Am. Chem. Soc.* **2011**, *133*, 16201−16211.
(28) Würthner, F. *Chem. Commun.* **2004**, 1564−1579.
(29) Görl, D.; Zhang, X.; Würthner, F. *Angew. Chem., Int. Ed.* **2012**, *51*, 6328−6348.
(30) Krieg, E.; Weissman, H.; Shirman, E.; Shimoni, E.; Rybtchinski, B. *Nat. Nanotechnol.* **2011**, *6*, 141−146.
(31) Gladysz, J. A.; Curran, D. P.; Horváth, I. T. *Handbook of fluorous chemistry*; Wiley-VCH: Weinheim, 2004.
(32) Krafft, M. P.; Riess, J. G. *Biochimie* **1998**, *80*, 489−514.
(33) Biffinger, J. C.; Kim, H. W.; DiMagno, S. G. *ChemBioChem* **2004**, *5*, 622−627.
(34) Dalvi, V. H.; Rossky, P. J. *Proc. Natl. Acad. Sci. U.S.A.* **2010**, *107*, 13603−13607.
(35) Mecinović, J.; Snyder, P. W.; Mirica, K. A.; Bai, S.; Mack, E. T.; Kwant, R. L.; Moustakas, D. T.; Héroux, A.; Whitesides, G. M. *J. Am. Chem. Soc.* **2011**, *133*, 14017−14026.
(36) Klebe, G.; Graser, F.; Hädicke, E.; Berndt, J. *Acta Crystallogr., Sect. B* **1989**, *45*, 69−77.
(37) Ghosh, S.; Li, X.-Q.; Stepanenko, V.; Würthner, F. *Chem.—Eur. J.* **2008**, *14*, 11343−11357.
(38) Chebotareva, N.; Bomans, P. H. H.; Frederik, P. M.; Sommerdijk, N. A. J. M.; Sijbesma, R. P. *Chem. Commun.* **2005**, 4967−4969.
(39) Leenders, C. M. A.; Albertazzi, L.; Mes, T.; Koenigs, M. M. E.; Palmans, A. R. A.; Meijer, E. W. *Chem. Commun.* **2013**, *49*, 1963−1965.
(40) Connolly, M. L. *J. Mol. Graph.* **1993**, *11*, 139−141.
(41) Klamt, A.; Schüürmann, G. *J. Chem. Soc., Perkin Trans. 2* **1993**, 799−805.
(42) Korth, M. *J. Chem. Theory Comput.* **2010**, *6*, 3808−3816.
(43) Graser, F.; Hädike, E. *Liebigs Ann. Chem.* **1984**, *1984*, 483−494.
(44) Skrabania, K.; Laschewsky, A.; Berlepsch, H. v.; Böttcher, C. *Langmuir* **2009**, *25*, 7594−7601.
(45) The complete set of aggregation curves, curve fitting, van't Hoff plots, and corresponding equations can be found in the Supporting Information.
(46) Van der Schoot, P. In *Supramolecular Polymers*; Ciferri, A., Ed.; CRC Press: Boca Raton, FL, 2005; pp 77−106.
(47) Smulders, M. M. J.; Schenning, A. P. H. J.; Meijer, E. W. *J. Am. Chem. Soc.* **2008**, *130*, 606−611.
(48) Filot, I. A. W.; Palmans, A. R. A.; Hilbers, P. A. J.; van Santen, R. A.; Pidko, E. A.; de Greef, T. F. A. *J. Phys. Chem. B* **2010**, *114*, 13667−13674.
(49) Ogi, S.; Sugiyasu, K.; Manna, S.; Samitsu, S.; Takeuchi, M. *Nat. Chem.* **2014**, *6*, 188−195.
(50) Li, Z.; Kesselman, E.; Talmon, Y.; Hillmyer, M. A.; Lodge, T. P. *Science* **2004**, *306*, 98−101.
(51) Meyer, E. A.; Castellano, R. K.; Diederich, F. *Angew. Chem., Int. Ed.* **2003**, *42*, 1210−1250.
(52) Pace, C. N. In *Enzyme Structure: Part L*; Colowick, N. P., Kaplan, N. P., Hirs, C. H. W., Timasheff, S. N., Eds.; Methods in Enzymology*131*, Academic Press: San Diego, CA, 1986; pp 266−280.
(53) Korevaar, P. A.; Schaefer, C.; de Greef, T. F. A.; Meijer, E. W. *J. Am. Chem. Soc.* **2012**, *134*, 13482−13491.
(54) Reichardt, C. *Solvents and solvent effects in organic chemistry*; Wiley-VCH: Weinheim, 2003.
(55) Chen, Z.; Fimmel, B.; Würthner, F. *Org. Biomol. Chem.* **2012**, *10*, 5845.
(56) Ortega, J.; Rafols, C.; Bosch, E.; Roses, M. *J. Chem. Soc., Perkin Trans. 2* **1996**, 1497.
(57) Dobrawa, R.; Würthner, F. *J. Polym. Sci., Part A: Polym. Chem.* **2005**, *43*, 4981−4995.
(58) Kurth, D. G.; Higuchi, M. *Soft Matter* **2006**, *2*, 915−927.
(59) Ben-Naim, A.; Mazo, R. *J. Phys. Chem. B* **1997**, *101*, 11221−11225.
(60) Jackson, R. M.; Sternberg, M. J. *Protein Eng.* **1994**, *7*, 371−383.